Adaptive tracking of a time-varying field with a quantum sensor

Cristian Bonato[1,*] and Dominic W. Berry[2]
[1]*Institute of Photonics and Quantum Sciences, SUPA, Heriot-Watt University, Edinburgh EH14 4AS, United Kingdom*
[2]*Department of Physics and Astronomy, Macquarie University, Sydney, NSW 2109, Australia*
(Received 27 March 2017; published 30 May 2017)

Sensors based on single spins can enable magnetic-field detection with very high sensitivity and spatial resolution. Previous work has concentrated on sensing of a constant magnetic field or a periodic signal. Here, we instead investigate the problem of estimating a field with nonperiodic variation described by a Wiener process. We propose and study, by numerical simulations, an adaptive tracking protocol based on Bayesian estimation. The tracking protocol updates the probability distribution for the magnetic field based on measurement outcomes and adapts the choice of sensing time and phase in real time. By taking the statistical properties of the signal into account, our protocol strongly reduces the required measurement time. This leads to a reduction of the error in the estimation of a time-varying signal by up to a factor of four compare with protocols that do not take this information into account.

DOI: 10.1103/PhysRevA.95.052348

I. INTRODUCTION

Sensors based on individual quantum objects, such as electrons or atoms, can enable measurements of physical quantities with very high spatial resolution [1]. Additionally, by exploiting quantum phenomena, one can reach a sensitivity beyond what is possible with classical techniques [2]. In the past decades, the exciting scientific progress in the control of quantum systems has led to the demonstration of quantum sensing protocols based on individual photons, electrons, etc. In this context, sensors based on single spins can map magnetic fields with nanometric spatial resolution, making them a revolutionary tool to study magnetic phenomena in nanoscale materials and biological processes [3,4]. The most prominent system in this field is the electronic spin associated with the nitrogen-vacancy (NV) center in diamond. Due to the weak spin-orbit coupling and an almost-spin-free ^{12}C environment, the NV center spin preserves quantum coherence on timescales much longer than the manipulation time. Remarkably, the spin can be read out at ambient conditions by optically detected magnetic resonance, making it a viable system for nanoscale magnetic sensing at ambient conditions.

These properties have led to ground-breaking experiments in nanoscale sensing, achieving a spatial resolution down to 10–20 nm [4], and a sensitivity sufficient to detect individual electron spins [5] and nanoscale volumes of nuclear spins [6–8] down to the individual nuclear spin level [9]. Remarkable experiments with NV centers include the application of nanoscale sensing to probe, for example, ballistic electron transport in a conductor [10], topological magnetic defects [11], spin waves [12], and vortices in superconducting materials [13,14].

The sensing capabilities of the NV electronic spin are not limited to magnetic fields but extend also to the measurement of other physical quantities such as temperature [15], electric fields [16], and strain [17]. Additionally, other defects in different materials, such as silicon carbide, exhibit sensing properties complementary to those of the NV center in diamond [18–21].

Quantum sensing experiments have mainly addressed the detection of constant (dc magnetometry) and periodic signals (ac magnetometry) [22]. For dc magnetometry a constant signal is estimated by detecting its effect on a coherent superposition, e.g., by measuring a spin rotation under an applied constant magnetic field. For ac magnetometry the amplitude and/or phase of a signal composed of one or a few harmonic tones is detected by applying echo sequences.

Reference [23] extended ac magnetometry to the reconstruction of nonperiodic waveforms by using a family of echo sequences that form a basis for the signal. Identical instances of the same signal are repeated and detected by using each echo sequence in the family, which allows the retrieval of specific Fourier coefficients. By combining all Fourier coefficients, corresponding to all the echo sequences in the family, the wave function can be reconstructed up to an arbitrary precision. This waveform reconstruction technique enables the reconstruction of fast oscillating waveforms but requires access to several identical instances of the same waveform in order to find the projection of the signal onto each echo sequence in the basis.

Here, we focus on a different problem: the reconstruction of a single instance of a time-varying magnetic field of known statistical properties. We propose a tracking protocol based on Bayesian estimation that extends a dc-magnetometry protocol to the estimation of a time-varying stochastic signal. We study the protocol performance in the case of a Wiener process and show that our protocol reduces the estimation time by up to a factor of four compared with known protocols in the literature, by taking the measurement history and the statistical properties of the signal into account. A different method for the related problem of measuring a phase that changes in discrete steps was presented in Ref. [24].

Our protocol may find applications for fast tracking of magnetic fields associated with diffusion processes; for example, in biology or in chemical reactions, or to track the Brownian motion of trapped magnetic nanoparticles. Additionally, this work could provide a faster way to track the dynamics of the spin bath surrounding the quantum sensor in the material. This could lead to a narrowing of the magnetic fluctuations and an increase of the spin coherence time [25,26].

*Corresponding author: c.bonato@hw.ac.uk

II. QUANTUM SENSING OVER A LARGE DYNAMIC RANGE

A. Single-spin dc magnetometry

In this section we summarize known techniques and results for measuring a constant frequency. A constant magnetic field B along the quantization axis z can be measured by detecting the rotation induced on a single spin (Ramsey experiment) in the xy plane. A spin initialized in the superposition state $(|0\rangle+|1\rangle)/\sqrt{2}$ evolves under B over time τ as $(|0\rangle+e^{i\gamma B\tau}|1\rangle)/\sqrt{2}$, where γ is the gyromagnetic ratio ($\gamma\sim 28$ MHz/mT for an electronic spin). Assuming perfect spin initialization and readout and no decoherence, the probability to detect the outcome $\mu\in\{0,1\}$ after time τ is

$$P(\mu|f_B)=\frac{1+(-1)^{\mu}\cos(2\pi f_B\tau+\theta)}{2}, \tag{1}$$

where $f_B=\gamma B/2\pi$. The phase θ corresponds to the rotation angle of the spin readout basis in the xy plane relative to the initialization state. The goal of a sensing experiment is to retrieve the frequency f_B with the highest possible accuracy over the largest possible range of values.

In realistic cases, the spin state associated with outcome μ can only be read out with finite fidelity ξ_μ, which is defined as the probability to detect μ given that the eigenstate corresponding to μ is prepared. Additionally, the coherence of the spin is limited by fluctuations of the magnetic environment, averaged over the sensing time. We include magnetic fluctuations induced by nuclear spins in the material as a Gaussian decoherence term described by the coherence time T_2^* [27]. In our following discussion, we assume T_2^* to be long ($T_2^*\sim 100\ \mu$s) so that we can focus on reconstructing the variation of the classical magnetic signal neglecting the fluctuations of the nuclear-spin environment. Coherence times of several hundred microseconds have been experimentally demonstrated in isotopically purified diamond samples [28,29].

Including finite readout fidelity and decoherence, Eq. (1) is modified to

$$P(\mu=0|f_B)=\frac{1+\xi_0-\xi_1}{2}+\frac{\xi_0+\xi_1-1}{2}e^{-(\tau/T_2^*)^2}\times\cos(2\pi f_B\tau+\theta), \tag{2}$$

and $P(\mu=1|f_B)=1-P(\mu=0|f_B)$. In the following, based on our previous experiment with resonant optical excitation of a NV center at cryogenic temperature [29], we assume good readout fidelity for the outcome $\mu=1$ ($\xi_1\sim 1$) and we only discuss the role of the readout fidelity for outcome $\mu=0$, which we simply denote ξ.

One fundamental issue with frequency estimation by Ramsey measurements is the trade-off between sensitivity and measurement range. In other words, there is a limit on the dynamic range, defined as the ratio between the maximum measurable frequency before saturation ($f_{\max}$) and the smallest detectable frequency, described by the uncertainty σ_f.

For a Ramsey experiment with sensing time τ repeated many times for total time T, the uncertainty σ_f decreases as $1/(2\pi\sqrt{\tau T})$. Therefore, the minimum uncertainty can be reached when measuring over the longest sensing time $\tau_{\max}$ before decoherence becomes significant, $\tau_{\max}\sim T_2^*$. On the other hand, the frequency range decreases with τ because the signal is periodic, creating ambiguity whenever $\|2\pi f_{\max}\tau\|>\pi$. As a result, the dynamic range is bounded as $f_{\max}/\sigma_f<\pi\sqrt{T/\tau}$.

Adaptive phase estimation protocols have been devised to overcome this limit. The basic idea is to probe the field with a combination of $K+1$ exponentially decreasing sensing times $\tau_k=2^k\tau_0$, where τ_0 is the smallest sensing time and $k=K,\ldots,0$ [30]. In adaptive measurements, the phase θ is adjusted based on the results of previous measurements. Provided there are multiple measurements for each sensing time, the uncertainty in estimating a phase scales as $1/N$, where N is the total number of applications of the phase shift [30].

Further developments also showed that adaptive feedback is not a strict requirement: nonadaptive protocols can reach $1/N$ scaling [31–33]. In the case of frequency estimation, this translates to an increase in the dynamic range to $f_{\max}/\sigma_f\sim\pi(T/\tau_0)$ [34–36]. For frequency estimation with realistic readout fidelity, it was initially found that nonadaptive protocols yielded the best results [37], but later improvements were found by using adaptive measurements [29,34].

These protocols, sketched in Fig. 1(a), use Bayesian estimation. The probability distribution $P(f_B)$ for the frequency f_B is assumed to be uniform at the beginning of each estimation sequence, then is updated after every Ramsey experiment according to Bayes' theorem. For the ℓth Ramsey in the estimation sequence, Bayes' theorem gives

$$P(f_B|\mu_1,\ldots,\mu_\ell)\propto P(f_B|\mu_1,\ldots,\mu_{\ell-1})P(\mu_\ell|f_B) \tag{3}$$

where $P(\mu_\ell|f_B)$ is given by Eq. (1). Although the frequency is not periodic, there are bounds to the range of possible values that will be considered, and the probability distribution for the frequency is periodic when multiples of τ_0 are used for the sensing time. It is therefore convenient to express the probability as a Fourier series

$$P(f_B)=\sum_j p_j e^{i2\pi j f_B\tau_0}. \tag{4}$$

The coefficients $\{p_j\}$ depend on the measurement results, but that dependence will not be shown for brevity.

In the remainder of this section we summarize methods and results from Ref. [32], except that we replace the phase with $2\pi f_B\tau_0$. When quantifying the performance of measurement of a periodic quantity, it is convenient to use the Holevo variance [38]. A modification of the Holevo variance, analogous to the mean-square error, is

$$V_H:=\langle\cos[2\pi(f_B-\hat{f}_B)\tau_0]\rangle^{-2}-1, \tag{5}$$

where $\hat{f}_B$ is the estimate of the frequency, and the average is over the actual frequency f_B and measurement results. This measure is convenient for designing the feedback protocol, but in this work we evaluate the performance of the estimation by the usual mean-square error. The best estimate for the frequency that minimizes V_H is given by

$$\hat{f}_B=\frac{1}{2\pi\tau_0}\arg\langle e^{i2\pi f_B\tau_0}\rangle, \tag{6}$$

where f_B on the right-hand side is a dummy variable for the Bayesian phase distribution, and the expectation value is over

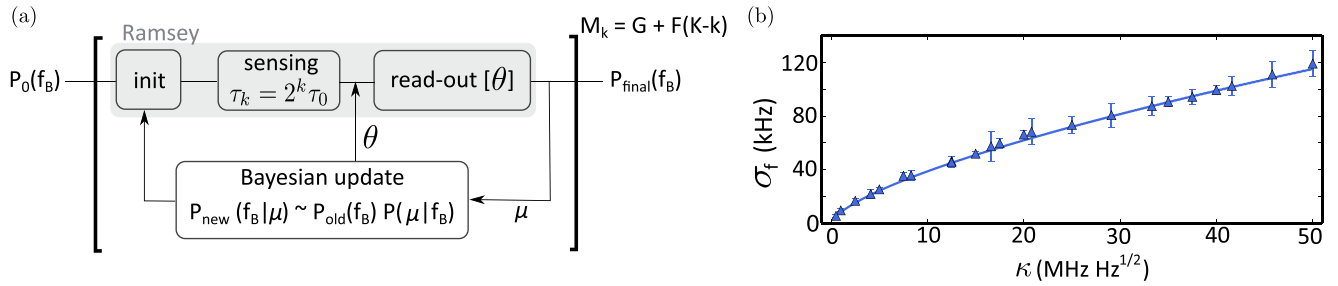

FIG. 1. (a) Conceptual diagram of the nontracking adaptive estimation protocol [29]. The protocol assumes an initial uniform distribution $P_0(f_B)$. Each Ramsey experiment, comprising spin initialization, a sensing time τ_k, and readout, generates an outcome μ which is used to update $P(f_B)$ through Bayes' theorem. After each Ramsey experiment, the current distribution $P(f_B)$ is used to calculate the controlled phase θ. Each Ramsey experiment, with sensing time τ_k, $k = K, \ldots, 0$ is repeated $M_k = G + (K-k)F$ times, where F, G are integers. At the end of the sequence, the frequency f_B is estimated from the final probability distribution $P_{\text{final}}(f_B)$, according to Eq. (6). (b) Error σ_f is plotted as a function of the fluctuation level κ [MHz Hz$^{1/2}$]. The points correspond to simulation results using the nontracking protocol for $G = 5$, $F = 3$. The curve shows the prediction of Eq. (16) with a fitted proportionality constant of 1.03.

that phase distribution. This estimate is very easily found from the Fourier coefficients as

$$\hat{f}_B = \frac{1}{2\pi\tau_0} \arg|p_{-1}|. \tag{7}$$

In addition, the value of $\langle\cos[2\pi(f_B - \hat{f}_B)\tau_0]\rangle$ in the expression for V_H can be found by averaging over $|\langle e^{i2\pi f_B\tau_0}\rangle|$. Using the Fourier representation of the probability distribution, this means that V_H is given by

$$V_H = (2\pi\langle|p_1|\rangle)^{-2} - 1, \tag{8}$$

where the expectation is now over the actual frequency and measurement results, and we have used $p_1 = p_{-1}^*$. This suggests the use of an adaptive sensing protocol, where the rotation of the spin readout basis θ is selected to maximize the expected value of $|p_1|$ after the next detection. That minimizes the value of V_H after the next detection.

The situation is more complicated, because initially large multiples of the interaction time τ_0 are used, which means that $p_1 = p_{-1} = 0$. When the smallest interaction time that has been used so far is $2^k\tau_0$, then one would instead replace τ_0 with $2^k\tau_0$ in the above discussion. In the approach of Ref. [30], one would choose θ to maximize $|p_{2^k}|$ after the next detection. If the smallest interaction time so far was $2^k\tau_0$, and a measurement to be performed is with an interaction time of $2^{k-1}\tau_0$, then it is better to minimize $|p_{2^{k-1}}|$ after the next detection. The appropriate value of θ to choose is then

$$\theta = \tfrac{1}{2}\arg(p_{-2^k}). \tag{9}$$

The adaptive technique for realistic readout fidelity in Ref. [29] uses this estimate in combination with a phase increment dependent only on the last measurement outcome, obtained by numerically optimizing the final variance for the specific experimental parameters through a swarm optimization procedure [34]. In this work, we use that method for the measurements without tracking of the phase. In contrast, for the measurements *with* tracking of the phase, we always use Eq. (9) to choose the controlled phase θ.

In the following, we describe the estimation error for f_B as the standard deviation based on the Holevo variance V_H [$\sigma_f = V_H^{1/2}/(2\pi\tau_0)$]. While here we follow the traditional approach of giving a point estimate and the variance, an alternative possibility would be to give credible intervals for the estimate [39]; for example, the frequency values f_1 and f_2 such that

$$P(f_1 < f_B < f_2|\mu_1 \ldots \mu_\ell) = 0.95. \tag{10}$$

Alternatively, in our Bayesian approach the probability distribution $P(f_B)$ is available at all times after each measurement: neglecting memory and data processing considerations, giving $P(f_B)$ would provide the experimenter with the most complete information.

Estimation error scaling as $\sigma_f \propto 2^{-K}/\tau_0$ cannot be achieved by using only a single repetition for each of the exponentially decreasing sensing times $2^k\tau_0$. However, the required bound can be reached by using a number of repetitions $M_k = G + (K-k)F$, where F, G are integers [29,31]. For the longest sensing time $2^K\tau_0$, a number G of repetitions is performed. The number of repetitions is then increased by F for each shorter sensing time. The additional number of repetitions for shorter sensing times removes the most detrimental errors, which correspond to measurements that make the largest distinction in frequency f_B. The total sensing time T for a single estimation sequence is

$$T = \tau_0[(2^{K+1} - 1)G + (2^{K+1} - K - 2)F], \tag{11}$$

which can be approximated by $T \sim (G + F)2^{K+1}\tau_0$ for large K.

B. Estimating a time-varying signal

Next we consider a frequency $f_B(t)$ varying according to a Wiener process

$$f_B(t + dt) = f_B(t) + \kappa d\mathcal{W}(t), \tag{12}$$

where $d\mathcal{W}(t)$ is an infinitesimal Wiener increment. It is defined such that the integral of $\mathcal{W}(t)$ for time Δt has mean zero and variance Δt. It can be simulated by discretizing time to intervals of length Δt and generating a normal distribution with variance Δt. The goal is to estimate $f_B(t)$ in real time with the smallest possible error. That is, we wish to estimate $f_B(t)$ at the current time by using data up to the current time.

The simplest way to estimate a time-varying field is to repeat the optimized adaptive protocol described in Sec. II A

and experimentally demonstrated in Ref. [29], which we will call the "nontracking protocol." The phase acquired during a Ramsey experiment, which for a constant f_B is simply $\varphi = 2\pi f_B \tau$ [as in Eq. (1)], becomes

$$\varphi = 2\pi \int_{t_0}^{t_0+\tau} f_B(t)dt. \tag{13}$$

As discussed in Sec. II A, for a constant f_B the minimum uncertainty is achieved by the longest sensing time $\tau_{\max}$ allowed by decoherence. In other words, the value of K shall be chosen so that the longest sensing time $\tau_{\max} = 2^K \tau_0$ is close to the spin coherence time T_2^*.

This choice of $\tau_{\max}$ is not necessarily optimal for a time-varying signal. In this case, the optimal K should be chosen such that the estimation error is similar to the change in signal over the measurement sequence (provided it is less than T_2^*). By choosing K larger than this, the signal would fluctuate over the measurement time by more than the measurement accuracy, resulting in an unreliable outcome. On the other hand, if K is smaller than necessary, then we would be restricting ourselves to a reduced accuracy. Therefore, we assume

$$\sigma_f \propto \kappa T^{1/2}, \tag{14}$$

where the total sensing time is $T \sim (G+F)2^{K+1}\tau_0$.

For a measurement scheme of this type the uncertainty σ_f should be inversely proportional to the total sensing time T. More specifically, the scaling should be as $\sigma_f \propto 1/(2^K\tau_0)$, but the constant of proportionality will depend on G and F. A rough approximation may be made by assuming that the constant of proportionality is $1/\sqrt{G}$. That is because the longest interaction time is repeated G times, and $1/\sqrt{G}$ is the scaling for measurements repeated G times. The measurements with shorter interaction times have more repetitions, but are primarily used for resolving ambiguities.

That means we should have the scaling

$$2^K\tau_0 \propto \frac{1}{[G(G+F)]^{1/3}\kappa^{2/3}}. \tag{15}$$

That then yields an uncertainty scaling as

$$\sigma_{\text{no-tr}} \propto \frac{(G+F)^{1/3}}{G^{1/6}}\kappa^{2/3}. \tag{16}$$

The important part of this expression is the scaling with $\kappa^{2/3}$, which is equivalent to the scaling that could be achieved for optical phase measurements with arbitrary squeezing [40–42]. We have performed numerical simulations of this nontracking protocol for $G = 5$, $F = 3$, and the results are shown in Fig. 1(b). There is excellent agreement with theory, and fitting for the proportionality constant for Eq. (16) yields $\sigma_{\text{no-tr}} = (1.03 \pm 0.04)\kappa^{2/3}$.

In the previous discussion we assumed that the estimation sequence only includes sensing time; i.e., all other operations, such as spin initialization, control, and readout are instantaneous. However, this is not true for realistic experiments, where all these operations contribute to an overhead time T_{OH}. A measurement sequence with $K+1$ different sensing times features a number of Ramsey experiments $R_K = (K+1)G + (K+1)KF/2$ [29], resulting in a total estimation time $T \sim (G+F)2^{K+1}\tau_0 + R_K T_{\text{OH}}$.

III. ADAPTIVE TRACKING

A. The algorithm

For a time-varying signal with known statistical properties, the available information can be exploited to shorten the estimation sequence. Given a frequency $f_B(t)$ at time t, the frequency at time $t+dt$ is likely to be not too distant from $f_B(t)$. Using the known signal statistics, one can reasonably predict a narrower frequency range for the next estimation, so it is not necessary to explore the whole range of possible values. In other words, instead of starting each estimation sequence from a uniform probability distribution, one could start from the Bayesian probability distribution from the prior measurements and take into account the variation of the frequency according to the signal statistics. This corresponds to tracking the time-varying signal.

Updating the probability distribution. For simplicity, we initially consider the case in which the frequency is constant. We also take the fidelities ξ_μ to be equal to 1. Then, given an outcome μ_ℓ for the ℓth Ramsey experiment, featuring a sensing time $\tau_k = 2^k\tau_0$, the update of the probability distribution corresponds to an update of the Fourier coefficients as

$$p_j^{(\ell)} = \frac{p_j^{(\ell-1)}}{2} + \frac{e^{-(\tau_k/T_2^*)^2}}{4}\left[e^{i(\mu_\ell\pi+\theta)}p_{j-2^k}^{(\ell-1)} + e^{-i(\mu_\ell\pi+\theta)}p_{j+2^k}^{(\ell-1)}\right]. \tag{17}$$

Over a small time interval δt, the change in frequency δf_B will have a normal distribution with variance $\kappa^2\delta t$:

$$P_G(\delta f_B) = \frac{1}{\sqrt{2\pi\delta t}\kappa}e^{-(\delta f_B)^2/(2\kappa^2\delta t)}. \tag{18}$$

Algorithm 1 Tracking protocol

$k = K$ (*sensing time index,* $\tau_k = 2^k\tau_0$)

while TRUE **do**

convolve ($\Delta t = 2^k\tau_0 + T_{\text{OH}}$) - [Eq. (20)]
calculate θ - [Eq. (9)]
$\mu =$ Ramsey ($\tau_k = 2^k\tau_0$, θ)
Bayesian update (μ, $2^k\tau_0$, θ) - [Eq. (17)]
calculate $\mathcal{F}$ - [Eq. (21)]

estimate f_B - [Eq. (7)]

if ($\mathcal{F} < \mathcal{F}^{(\text{thr})}[k]$) **then**
  if ($k < K$) **then**
    $k = k + 1$
  end if
else
  if $k > 0$ **then**
    $k = k - 1$
  end if
end if
end while

Ignoring any information from a measurement, the probability distribution for the frequency after a time δt will be the convolution of the initial probability distribution with the Gaussian in Eq. (18), giving

$$P^{(\ell)}(f_B) = \int P^{(\ell-1)}(f_B - \nu) P_G(\nu) d\nu = \sum_j p_j e^{-2(\pi j \kappa \tau_0)^2 \delta t} e^{i 2\pi j f_B \tau_0}. \quad (19)$$

Therefore, the coefficients $p_k^{(\ell)}$ for the probability distribution after a time δt (without measurement) can be calculated as

$$p_j^{(\ell)} = p_j^{(\ell-1)} e^{-2(\pi j \kappa \tau_0)^2 \delta t}. \quad (20)$$

Provided the frequency does not vary significantly during an interaction time, the probability distribution may be approximated by using Eqs. (17) and (20) independently. Using this approach the simulations still accurately model measurements made by using this technique. An exact calculation of the probability distribution could potentially result in more accurate estimates, but the method to perform such a calculation appears to be an open question.

The adaptive tracking protocol. The tracking protocol is described by the pseudocode in Algorithm 1. Each estimation sequence uses a probability distribution $P(f_B)$ based on the previous measurements. As before, Ramsey experiments are performed by starting from the longest sensing time $2^K \tau_0$, and updating the probability distribution $P(f_B)$ according to Bayes' theorem. The difference is that now, instead of using all sensing times τ_k with $G + (K-k)F$ repetitions, the protocol adaptively chooses the best sensing time for each estimation, starting from the longest sensing time $2^K \tau_0$. To judge the accuracy of the estimate with sensing time τ_k, a figure of merit $\mathcal{F}$ is calculated based on the Bayesian probability distribution and compared with a threshold $\mathcal{F}^{(\mathrm{thr})}[k]$. If the figure of merit satisfies $\mathcal{F} < \mathcal{F}^{(\mathrm{thr})}[k]$ then the sensing time is increased to τ_{k+1} for the next estimation. If the estimate is not sufficiently accurate, then the sensing time for the next estimation is reduced to τ_{k-1}. At that point, if the threshold is satisfied for the new estimation, the sensing time is increased back to τ_k. Otherwise, if the threshold is not satisfied, then the sensing time is further reduced to τ_{k-2}, and so on. While the nontracking protocol requires a large number of Ramsey experiments for each estimation, the adaptive tracking protocol outputs an estimation of the time-varying field for each Ramsey experiment.

We choose as a figure of merit $\mathcal{F}$ an estimate of the standard deviation of the probability distribution, which can be retrieved from the Holevo variance as

$$\mathcal{F} = \frac{V_H^{1/2}}{2\pi\tau_0} = \frac{1}{2\pi\tau_0}[(2\pi|p_{-1}|)^{-2} - 1]^{1/2}. \quad (21)$$

This expression only depends on the coefficient p_{-1} and can easily be calculated in real time. The estimation error is expected to scale as $\sigma_f \propto 2^K/\tau_0$. Therefore, we set the threshold corresponding to the sensing time $2^k\tau_0$ to be

$$\mathcal{F}^{(\mathrm{thr})}[k] = \frac{\alpha}{2^k \tau_0}. \quad (22)$$

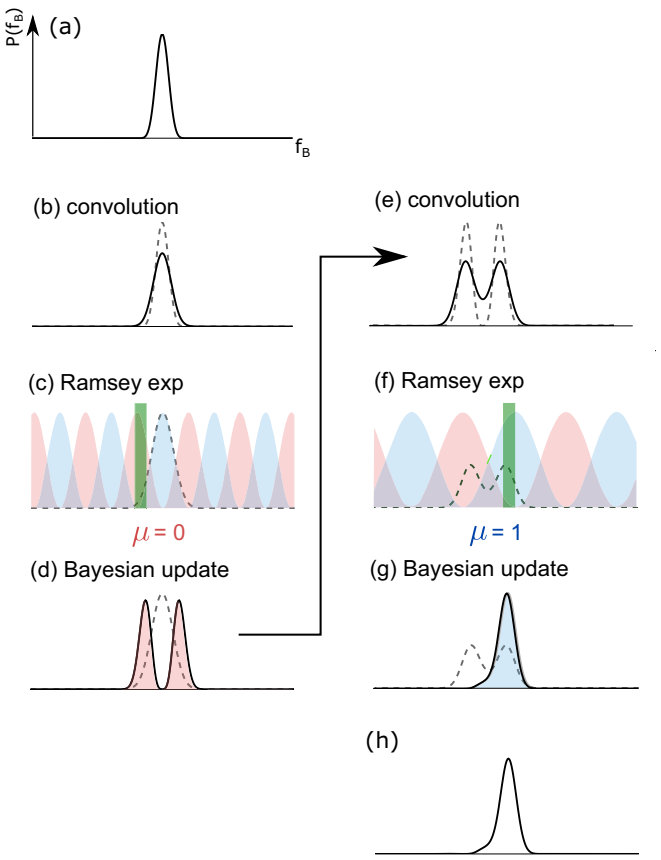

FIG. 2. Example of one estimation sequence for the tracking protocol described by the pseudocode in Algorithm 1. (a) The probability density for the current field estimation is (b) convolved with the expected variation over the measurement time. A Ramsey experiment is performed: each of the two outcomes ($\mu = 0,1$) is associated with a conditional probability $P(\mu|f_B)$, represented, respectively, by red and blue shaded areas in panel (c). The outcome $\mu = 0$ leads to the probability distribution $P'(f_B) \sim P_0(f_B)P(\mu{=}0|f_B)$ in panel (d). The figure of merit $\mathcal{F}$ for the two-peak distribution in panel (e) is below threshold and (f) a new measurement is performed with a shorter sensing time, after a new convolution step, to (g) discriminate between the two peaks. The outcome $\mu = 1$ leads to a narrow single-peaked distribution with figure of merit $\mathcal{F}$ above the threshold, which can be taken as a new estimate of f_B. The green vertical lines correspond to the actual values of f_B at the specific time of each operation. Solid (dashed) black lines represent the current (previous) form of the probability distribution $P(f_B)$.

Numerical simulations suggest that the optimal value for the proportionality factor α is 0.15.

This protocol is adaptive in two ways. First of all, it chooses in real time the measurement phase according to Eq. (9). Second, it adapts the sensing time at each step, based on the current estimated variance. As a consequence, while the nontracking protocol requires an optimal choice of K for optimal performance (Sec. II B) and suboptimal choices of K lead to large estimation errors, the tracking protocol is very robust and automatically selects the proper value of k at each step.

An example of the working principles of the tracking protocol can be found in Fig. 2. Examples of reconstructions of time-varying fields with the tracking protocol, as compared

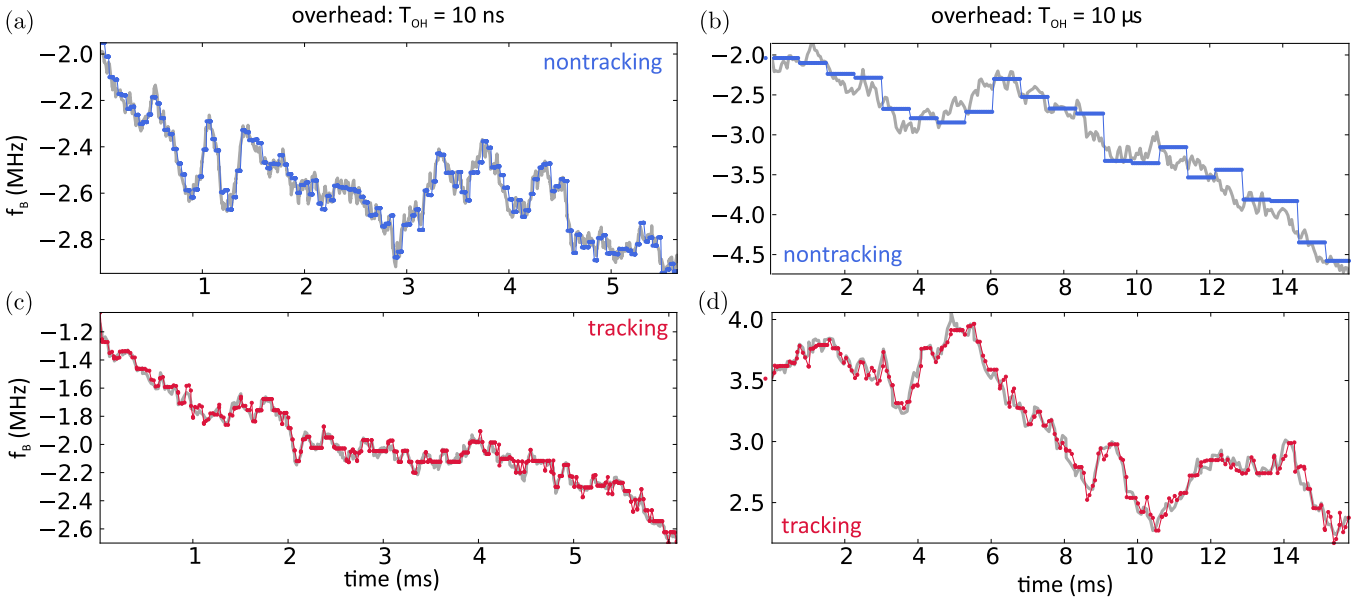

FIG. 3. Examples of waveforms (lighter-color curves, in gray) reconstructed with the nontracking [(a) and (b), darker (blue) curves] and tracking [(c) and (d), darker (red) curves] protocols. On the left side, for (a) and (c), the overhead is small ($T_{\rm OH} = 10$ ns) and the measurement time mostly consists of the Ramsey sensing time. In this case, the improvement by the tracking protocol is minimal. On the right side, for (b) and (d), when the overhead due to spin initialization and readout is more significant ($T_{\rm OH} = 10\ \mu$s), the advantage of the tracking protocol is clear. In all plots, the time-varying signal $f_B(t)$ (lighter gray curves) evolves according to a Wiener process described by Eq. (12).

with the nontracking protocol described in Sec. II B, are shown in Fig. 3. The nontracking protocol can successfully estimate time-varying parameters, with no previous knowledge of the properties of the signal. When the overhead is small [Figs. 3(a) and 3(c)], the performance of the nontracking and tracking protocols appears to be similar. The advantage of the tracking protocol in following fast signal variations is clearly evident when overhead is large [Figs. 3(b) and 3(d), for $T_{\rm OH} = 10\ \mu$s].

B. Performance estimation

The shortest estimation sequence for the tracking protocol would be to simply repeat the longest sensing time $\tau_{\rm max} = 2^K\tau_0$ once, so that the estimation error scales as

$$\sigma_f \propto \frac{1}{2^K\tau_0}. \tag{23}$$

Requiring that the variation of the frequency during a total sensing time of $2^K\tau_0$ is comparable to the uncertainty leads to the scaling

$$\sigma_{\rm tr} \propto \kappa^{2/3}. \tag{24}$$

If we assume that the scaling constant is 1, the ratio η between the errors in the nontracking and tracking cases is

$$\eta = \frac{\sigma_{\rm no-tr}}{\sigma_{\rm tr}} = \frac{(G+F)^{1/3}}{G^{1/6}}. \tag{25}$$

For $G = 5$, $F = 3$, we obtain $\eta \sim 1.5$. The improvement expected for the tracking protocol is modest, and in simulations there is not a large difference, as illustrated by the time-domain waveforms on the left side of Fig. 3. The reason for this is that the primary mechanism for improving the performance is using the prior information to resolve ambiguities, instead of measurements with shorter sensing times. This means we can save the time used for the shorter measurements and instead use the measurements with longer sensing times. However, the contribution to the total time from the measurements with shorter interaction times is not large. The longest sensing time $2^K\tau_0$ is almost the same as the sum of all the other sensing times $2^{K-1}\tau_0, \ldots, 2^0\tau_0$, which means that the tracking protocol does not dramatically shorten the total estimation time.

A more consistent improvement can be expected when taking overhead into account. In the limit of large overhead, the major contribution to the estimation time is given by the overhead, while the sensing time can be neglected. The estimation time for the tracking protocol can be approximated by $T_{\rm OH}$, as compared with $T \sim [(K+1)G + (K+1)KF/2]T_{\rm OH}$ for the nontracking protocol. As an example, if $T_{\rm OH} = 100\ \mu$s, the tracking protocol delivers an estimation every 100 μs. In contrast, the nontracking protocol performs one estimation every 1.24 ms (assuming $G = 5$, $F = 3$, $K = 7$). Since the estimation error scales as the square root of the estimation time [see Eq. (14)], we expect an improvement on the order of $\eta \sim [(1.24\ {\rm ms})/(100\ \mu{\rm s})]^{1/2}$, corresponding to a factor 3–4.

C. Numerical simulations

The performance of the two protocols has been tested by numerical simulations, for a range of parameter values. We select the minimum sensing time $\tau_0 = 20$ ns, corresponding to a frequency range $f_B \in [-25, +25]$ MHz. An instance of a time-varying signal $f_B(t)$ is produced according to the Wiener process in Eq. (12), starting from a random value for $f_B(0)$, with a temporal resolution of $\tau_0 = 20$ ns. To avoid values out of the $[-25, +25]$ MHz range, the waveform is truncated if $|f_B| > 24$ MHz. The signal $f_B(t)$ is reconstructed by using either protocol, providing the reconstructed waveform $\hat{f}_B(t)$. To evaluate the performance of the estimation, we use the

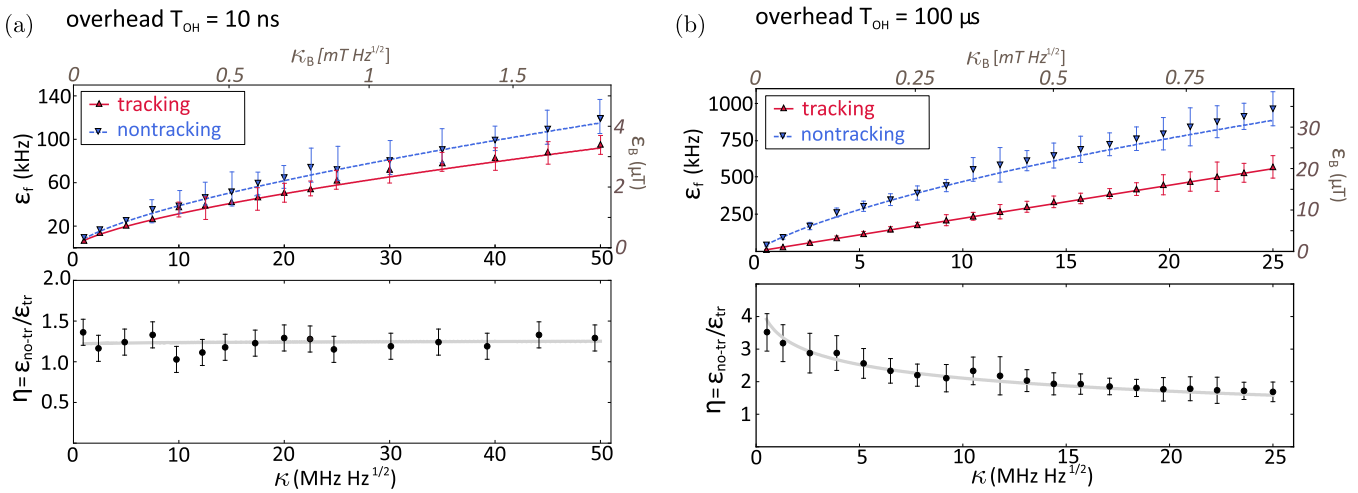

FIG. 4. Comparison between the performances of the nontracking and tracking protocols in (a) the limit of small overhead and (b) large overhead, for perfect readout fidelity $\xi = 1$. In the upper graphs, the points show the waveform estimation error ε_f for the tracking (upward-pointing triangles, red) and nontracking (downward-pointing triangles, blue) protocols, as a function of κ, from numerical simulations. The lines (solid for tracking, dashed for nontracking) are the theoretical predictions based on Eqs. (16) and (24), respectively, with the proportionality factors obtained by fitting. The gray axes on top and on the right show the same quantities specified for the case of a magnetic-field sensor, representing κ_B in [mT Hz$^{1/2}$] and the waveform estimation error in μT, respectively. In the lower graphs, the ratio η between the waveform estimation errors for the nontracking and tracking cases is shown.

mean-square error

$$\varepsilon^2 = \frac{1}{T}\int_0^T |f_B(t) - \hat{f}_B(t)|^2 dt. \tag{26}$$

Simulation results for the limit of negligible overhead ($T_{\rm OH} = 10$ ns) are shown in Fig. 4(a). On the top plot, the tracking algorithm (blue downward-pointing triangles) exhibits a relatively small improvement compared with the the nontracking algorithm (red upward-pointing triangles), by a factor of $\eta = 1.23 \pm 0.09$, similar to the theoretical prediction $\eta \sim 1.5$ in the previous section.

The case of longer overhead is shown in Fig. 4(b). As hinted by the reconstructed waveforms in Fig. 3, the advantage is here more significant, reaching $\eta \sim 3$–4. Given the different approximations used, the theoretical predictions based on Eq. (14) agree surprisingly well with the results of the numerical simulations.

The role of the overhead time is investigated in more detail by examining the protocols' performances for a fixed value of κ ($\kappa = 2$ MHz Hz$^{1/2}$), while sweeping the overhead time $T_{\rm OH}$ between 0 and 300 μs. The results are plotted in Fig. 5. The improvement given by the tracking protocol (described by η) is small for small overhead, as already evidenced in Fig. 4. For larger overhead, η is larger, up to about a factor of three and it is roughly independent of $T_{\rm OH}$, as predicted in Sec. III B.

In the last set of numerical simulations (Fig. 6), we illustrate the effect of a reduced spin readout fidelity ξ. We compare the waveform estimation error ε_f for the nontracking and tracking protocols for $\xi = 0.75$ and $\xi = 0.88$. The latter value corresponds to the fidelity of spin readout for the experimental demonstration in Ref. [29]. Reduced readout fidelity leads, as one can expect, to an increase in the estimation error. The ratio η, however, does not vary significantly.

IV. EXPERIMENTAL OUTLOOK

Our analysis has been restricted to the case when the classical spin readout noise is smaller than the spin projection noise; i.e., when "single-shot" readout is available. Currently, single-shot readout has only been experimentally demonstrated by exploiting resonant optical excitation of spin-dependent transitions at cryogenic temperature [43]. This technique features high-fidelity spin initialization (fidelity >0.99) and readout (fidelities $\xi_1 \sim 0.99$ and $\xi_0 > 0.9$). The requirement of cryogenic operation is, however, a serious restriction for applications to quantum sensing. Recent experiments have shown some promise towards the demonstration of single-shot readout at room temperature. A first approach involves spin-to-charge

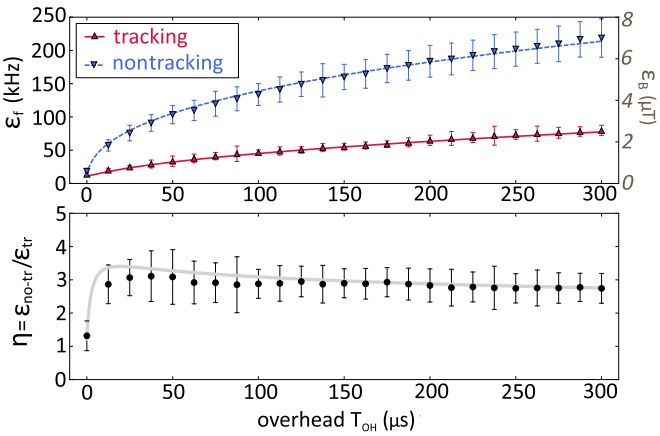

FIG. 5. Protocol performance as a function of the measurement overhead (qubit initialization and readout time), for a fixed value for $\kappa = 2$ MHz Hz$^{1/2}$. On the bottom graph, the ratio η between the waveform estimation errors for the nontracking and tracking protocols is shown.

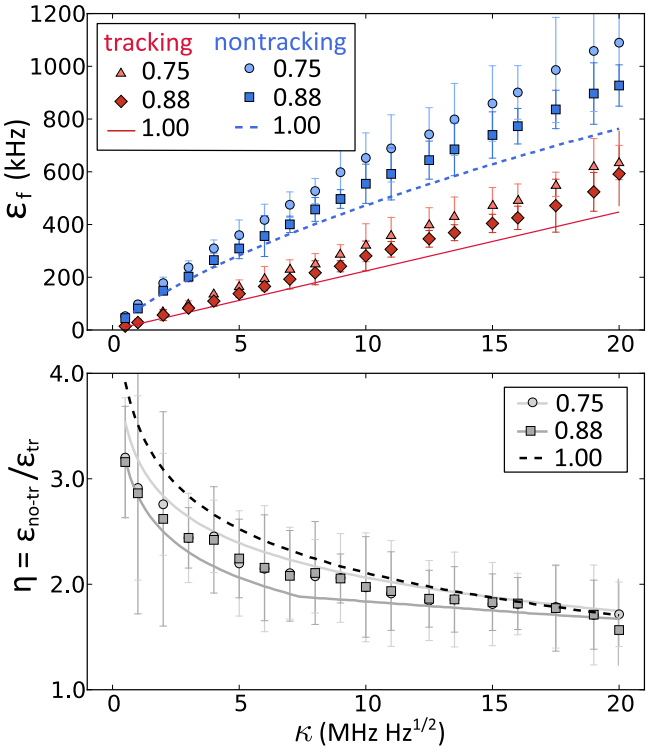

FIG. 6. Protocol performance for finite readout fidelity ξ in the nontracking (blue points, squares for $\xi = 0.88$ and circles for $\xi = 0.75$) and tracking cases (red points, diamonds for $\xi = 0.88$ and triangles for $\xi = 0.75$). Lines (solid red line for tracking, dashed blue line for nontracking) correspond to the estimation error in the case of perfect fidelity ($\xi = 1$). For all plots, the overhead is $T_{\mathrm{OH}} = 100\ \mu$s. On the bottom graph, the ratio η between the waveform estimation errors for the nontracking and tracking protocols is shown, for $\xi = 0.75$ (circles) and $\xi = 0.88$ (squares).

conversion by optical ionization and successive detection of the defect charging state [44,45]. This approach may be further enhanced by the integration of electrical contacts to provide photoelectric spin readout [46]. A second approach involves the storage of the electron-spin population onto the nuclear spin, which can be read out several times through the electron spin itself [47]. In both cases, a large overhead is introduced, which provides further motivation for our analysis.

Typically, the NV center spin is read out at room temperature by spin-dependent photoluminescence intensity, originating from spin-dependent decay rates through a metastable state under optical excitation (optically detected magnetic resonance). In contrast to the "single-shot" readout case, the readout noise is here larger than the spin projection noise and spin readout must be repeated several times for each sensing time. A large number of repetitions ($\sim 10^5$ for a typical experiment with NV centers) can be seen as a large overhead, suggesting that our tracking protocol will also be useful for such experiments.

In this work, we discussed the specific case of a time-varying signal described by a Wiener process, assuming that the parameter κ is known. In case κ is not known, one could simply start by measuring the signal evolution with the nontracking protocol and retrieving an estimate of κ that can be used for tracking at a later stage. Additionally, our approach is quite general and can be easily extended to other kinds of stochastic processes. Particularly relevant is the Ornstein–Uhlenbeck process [27], which describes the fluctuations of a nuclear-spin bath in the semiclassical approximation.

An interesting extension of this work would be to the case of the magnetic field induced by a quantum bath, such as the nuclear-spin bath. If the correlation time of the bath dynamics is long enough, each estimation sequence provides a projective measurement of the magnetic field originating from the bath. The backaction of such a projective measurement would narrow the probability distribution for the magnetic field induced by the bath, leading to an extension of the spin coherence time T_2^* [25,26]. By providing faster field estimation, our protocol could allow us to partially relax the requirement of long bath correlation time and slow dynamics. Additionally, spin readout by optical excitation can induce perturbations in the bath by causing unwanted electron-spin flips that affect the bath through the hyperfine interaction. By reducing the number of readouts required for each estimation, a reduction of unwanted bath perturbations induced by optical spin readout can be expected.

In addition to extending the sensor coherence time, the measurement backaction on the spin bath could also be used as a state preparation tool. For weakly coupled nuclear spins in the bath, each Ramsey experiment in the estimation sequence acts as a weak spin measurement. It has been shown that a sequence of weak measurements with sensing times which are adapted in real time can be used as a tool for spin preparation [48,49]. It would be interesting to investigate whether the tracking protocol could be adapted to provide, at the same time, the preparation of predetermined quantum states of the bath.

A different research direction could be to extend this work to the spatial domain, to the field of microscopy. The acquisition of a bidimensional image requires considerable time, over which the system must be stable against fluctuations and drifts, posing a technological challenge. In this case, any *a priori* knowledge of the statistical properties and correlation scales of the image could be used to speed up the measurement process [50].

V. CONCLUSIONS

In this work, we discussed the measurement of a single instance of a time-varying field, of known statistical properties, with a quantum sensor. We investigated the performance of a nontracking protocol, previously considered only for constant fields, which does not use any information about the signal. Through numerical simulations, we showed that the protocol can successfully track a time-varying field. We introduced a tracking protocol based on Bayesian estimation. By using the additional information about the statistical properties of the signal, the tracking protocol shortens the time required for each estimation, leading to a reduced measurement uncertainty in the estimation of a time-varying field. While a small improvement is achieved when including only the sensing time, a considerable reduction in the estimation error, up to four times, is shown when taking the realistic measurement overhead (spin initialization and readout time) into account. Our findings can be relevant for fast tracking of time-varying magnetic fields associated with diffusion processes in biology and materials science.

ACKNOWLEDGMENTS

The authors thank Machiel S. Blok, Hossein T. Dinani, Dale Scerri, and Erik Gauger for helpful discussions. D.W.B. is funded by an Australian Research Council Discovery Project (DP160102426).

[1] C. L. Degen, F. Reinhard, and P. Cappellaro, arXiv:1611.02427 (2016).
[2] V. Giovannetti, S. Lloyd, and L. Maccone, Nat. Photon. **5**, 222 (2011).
[3] R. Schirhagl, K. Chang, M. Loretz, and C. L. Degen, Annu. Rev. Phys. Chem. **65**, 83 (2014).
[4] J. Wrachtrup and A. Finkler, J. Magn. Reson. **269**, 225 (2016).
[5] M. S. Grinolds, M. Warner, K. D. Greve, Y. Dovzhenko, L. Thiel, R. L. Walsworth, S. Hong, P. Maletinsky, and A. Yacoby, Nat. Nanotechnol. **9**, 279 (2014).
[6] D. Rugar, H. J. Mamin, M. H. Sherwood, M. Kim, C. T. Rettner, K. Ohno, and D. D. Awschalom, Nat. Nanotechnol. **10**, 120 (2015).
[7] T. Häberle, D. S.-Lorch, F. Reinhard, and J. Wrachtrup, Nat. Nanotechnol. **10**, 125 (2015).
[8] S. J. DeVience, L. M. Pham, I. Lovchinsky, A. O. Sushkov, N. Bar-Gill, C. Belthangady, F. Casola, M. Corbett, H. Zhang, M. Lukin, H. Park, A. Yacoby, and R. L. Walsworth, Nat. Nanotechnol. **10**, 129 (2015).
[9] C. Müller, X. Kong, J.-M. Cai, K. Melentijević, A. Stacey, M. Markham, D. Twitchen, J. Isoya, S. Pezzagna, J. Meijer, J. F. Du, M. B. Plenio, B. Naydenov, L. P. McGuinness, and F. Jelezko, Nat. Commun. **5**, 4703 (2014).
[10] S. Kolkowitz, A. Safira, A. A. High, R. C. Devlin, S. Choi, Q. P. Unterreithmeier, D. Patterson, A. S. Zibrov, V. E. Manucharyan, H. Park, and M. D. Lukin, Science **347**, 1129 (2015).
[11] A. Dussaux, P. Schoenherr, K. Koumpouras, J. Chico, K. Chang, L. Lorenzelli, N. Kanazawa, Y. Tokura, M. Garst, A. Bergman, C. L. Degen, and D. Meier, Nat. Commun. **7**, 12430 (2016).
[12] T. van der Sar, F. Casola, R. Walsworth, and A. Yacoby, Nat. Commun. **6**, 7886 (2015).
[13] L. Thiel, D. Rohner, M. Ganzhorn, P. Appel, E. Neu, B. Müller, R. Kleiner, D. Koelle, and P. Maletinsky, Nat. Nanotechnol. **11**, 677 (2016).
[14] M. Pelliccione, A. Jenkins, P. Ovartchaiyapong, C. Reetz, E. Emmanouilidou, N. Ni, and A. C. Bleszynski Jayich, Nat. Nanotechnol. **11**, 700 (2016).
[15] G. Kucsko, P. C. Maurer, N. Y. Yao, M. Kubo, H. J. Noh, P. K. Lo, H. Park, and M. D. Lukin, Nature (London) **500**, 54 (2013).
[16] F. Dolde, H. Fedder, M. W. Doherty, T. Nöbauer, F. Rempp, G. Balasubramanian, T. Wolf, F. Reinhard, L. C. L. Hollenberg, F. Jelezko, and J. Wrachtrup, Nat. Phys. **7**, 459 (2011).
[17] M. W. Doherty, V. V. Struzhkin, D. A. Simpson, L. P. McGuinness, Y. Meng, A. Stacey, T. J. Karle, R. J. Hemley, N. B. Manson, L. C. L. Hollenberg, and S. Prawer, Phys. Rev. Lett. **112**, 047601 (2014).
[18] A. L. Falk, P. V. Klimov, B. B. Buckley, V. Ivády, I. A. Abrikosov, G. Calusine, W. F. Koehl, A. Gali, and D. D. Awschalom, Phys. Rev. Lett. **112**, 187601 (2014).
[19] H. Kraus, V. A. Soltamov, F. Fuchs, D. Simin, A. Sperlich, P. G. Baranov, G. V. Astakhov, and V. Dyakonov, Sci. Rep. **4**, 5303 (2014).
[20] M. Niethammer, M. Widmann, S.-Y. Lee, P. Stenberg, O. Kordina, T. Ohshima, N. T. Son, E. Janzén, and J. Wrachtrup, Phys. Rev. Appl. **6**, 034001 (2016).
[21] C. J. Cochrane, J. Blacksberg, M. A. Anders, and P. M. Lenahan, Sci. Rep. **6**, 37077 (2016).
[22] J. M. Taylor, P. Cappellaro, L. Childress, L. Jiang, D. Budker, P. R. Hemmer, A. Yacoby, R. Walsworth, and M. D. Lukin, Nat. Phys. **4**, 810 (2008).
[23] A. Cooper, E. Magesan, H. N. Yum, and P. Cappellaro, Nat. Commun. **5**, 3141 (2014).
[24] N. Wiebe and C. E. Granade, Phys. Rev. Lett. **117**, 010503 (2016).
[25] P. Cappellaro, Phys. Rev. A **85**, 030301 (2012).
[26] M. D. Shulman, S. P. Harvey, J. M. Nichol, S. D. Bartlett, A. C. Doherty, V. Umansky, and A. Yacoby, Nat. Commun. **5**, 5156 (2014).
[27] G. de Lange, Z. H. Wang, D. Risté, V. V. Dobrovitski, and R. Hanson, Science **330**, 60 (2010).
[28] G. Balasubramanian, P. Neumann, D. Twitchen, M. Markham, R. Kolesov, N. Mizuochi, J. Isoya, J. Achard, J. Beck, J. Tissler, V. Jacques, P. R. Hemmer, F. Jelezko, and J. Wrachtrup, Nat. Mater. **8**, 383 (2009).
[29] C. Bonato, M. S. Blok, H. T. Dinani, D. W. Berry, M. L. Markham, D. J. Twitchen, and R. Hanson, Nat. Nanotechnol. **11**, 247 (2016).
[30] B. L. Higgins, D. W. Berry, S. D. Bartlett, H. M. Wiseman, and G. J. Pryde, Nature (London) **450**, 393 (2007).
[31] B. L. Higgins, D. W. Berry, S. D. Bartlett, M. W. Mitchell, H. M. Wiseman, and G. J. Pryde, New J. Phys. **11**, 073023 (2009).
[32] D. W. Berry, B. L. Higgins, S. D. Bartlett, M. W. Mitchell, G. J. Pryde, and H. M. Wiseman, Phys. Rev. A **80**, 052114 (2009).
[33] K. M. Svore, M. B. Hastings, and M. Freedman, Quantum Inf. Comput. **14**, 306 (2013).
[34] A. J. F. Hayes and D. W. Berry, Phys. Rev. A **89**, 013838 (2014).
[35] G. Waldherr, J. Beck, P. Neumann, R. S. Said, M. Nitsche, M. L. Markham, D. J. Twitchen, J. Twamley, F. Jelezko, and J. Wrachtrup, Nat. Nanotechnol. **7**, 105 (2014).
[36] N. M. Nusran, U. Momeen, and M. V. G. Dutt, Nat. Nanotechnol. **7**, 109 (2012).
[37] R. S. Said, D. W. Berry, and J. Twamley, Phys. Rev. B **83**, 125410 (2011).
[38] A. S. Holevo, Springer Lect. Notes Math. **1055**, 153 (1984).
[39] D. S. Sivia, *Data Analysis: A Bayesian Tutorial* (Oxford University Press, Oxford, 2006).
[40] D. W. Berry and H. M. Wiseman, Phys. Rev. A **65**, 043803 (2002).
[41] D. W. Berry and H. M. Wiseman, Phys. Rev. A **73**, 063824 (2006).
[42] D. W. Berry and H. M. Wiseman, Phys. Rev. A **87**, 019901(E) (2013).

[43] L. Robledo, L. Childress, H. Bernien, B. Hensen, P. F. A. Alkemade, and R. Hanson, Nature (London) **477**, 574 (2011).
[44] B. J. Shields, Q. P. Unterreithmeier, N. P. D. Leon, H. Park, and M. D. Lukin, Phys. Rev. Lett. **114**, 136402 (2015).
[45] D. A. Hopper, R. R. Grote, A. L. Exarhos, and L. C. Bassett, Phys. Rev. B **94**, 241201 (2016).
[46] E. Bourgeois, A. Jarmola, P. Siyushev, M. Gulka, J. Hruby, F. Jelezko, D. Budker, and M. Nesladek, Nat. Commun. **6**, 8577 (2015).
[47] T. Häberle, T. Oeckinghaus, D. S.-Lorch, M. Pfender, F. Favaro de Oliveira, S. A. Momenzadeh, A. Finkler, and J. Wrachtrup, Rev. Sci. Instrum. **88**, 013702 (2017).
[48] M. S. Blok, C. Bonato, M. L. Markham, D. J. Twitchen, V. V. Dobrovitski, and R. Hanson, Nat. Phys. **10**, 189 (2014).
[49] J. N. Greiner, D. B. R. Dasari, and J. Wrachtrup, Sci. Rep. **7**, 529 (2017).
[50] M. Singh, K. Khare, A. K. Jha, S. Prabhakar, and R. P. Singh, Phys. Rev. A **91**, 021802 (2015).